




Investigation of the mechanical properties of Inconel 718 and AISI 316L welded materials using continuous drive friction welding

Ömer Karabey^{1*}, Ahmet Akkuş², Mehmet Akif Hafızoğlu³

¹Bitlis Eren University – Mechanical Engineering, 13100, Bitlis, Türkiye

²Sivas Cumhuriyet University – Mechanical Engineering, 58140, Sivas, Türkiye

³Dicle University – Mechanical Engineering, 21280, Diyarbakır, Türkiye

Received 31 January 2025, received in revised form 7 October 2025, accepted 29 October 2025

Abstract

In this study, Inconel 718 and AISI 316L were joined by continuous drive friction welding (CDFW) with 27 different welding parameter combinations. After welding the specimens with these 27 parameters, microstructural analyses were first carried out using an Optical Microscope (OM), a Scanning Electron Microscope (SEM), and Energy-Dispersive Spectrometry (EDS). Later, mechanical property investigations included hardness and tensile tests. Moreover, hardness distributions were analyzed from the cross-section of the welded specimens. Besides, the maximum tensile strength was obtained as 736.3 MPa, and the minimum tensile strength was obtained as 653.6 MPa in all cases. Consequently, friction welding of these dissimilar materials without any heat treatment was found to be applicable. It was also concluded that the most appropriate welding parameters among the 27 welding parameter combinations were 1600 rpm, 6 s friction time, and 40 MPa friction pressure.

Key words: continuous drive friction welding, dissimilar materials, hardness, superalloy, Inconel 718, AISI 316L

1. Introduction

Many different materials are required for today's needs. In many industrial applications, these different materials should be used in conjunction. To connect these different materials simultaneously, mechanical or welded connections are generally preferred. Welded connections are preferred over mechanical connections because they are easier and faster to install. There are many methods for welded joints in the literature, such as fusion welding and solid-state welding (SSW). In fusion welding, it is very difficult to join materials, especially dissimilar materials, without disturbing their mechanical properties. Therefore, different welding methods have been developed [1]. One of the most commonly used welding methods is friction welding. This method has attracted considerable attention in modern manufacturing due to its ability to form strong bonds between dissimilar materials. Un-

like conventional fusion welding, friction welding requires no melting of the materials. Besides, the friction welding method produces stronger joints without the use of additional filler material by applying controlled mechanical friction. This unique characteristic property eliminates the risk of solidification defects and reduces the area of the Heat-Affected Zone (HAZ). Thanks to these advantages, the friction welding method is an appealing choice for various applications, including the aerospace, automotive, and energy industries [2, 3].

The fundamentals of friction welding involve the rubbing of two workpieces together under high pressure. As a result, localized heating occurs at the interface of the materials, and the materials are plastically deformed. Then, an axial or rotational force is applied to the materials being rubbed. In this way, the softened materials resulting from frictional heating during rubbing form a metallurgical bond, which ex-

*Corresponding author: e-mail address: okarabey@beu.edu.tr

hibits extraordinary mechanical properties and structural integrity [4–6]. There exist several kinds of friction welding methods. One of them is Linear Friction Welding (LFW). LFW involves the relative motion of two workpieces along a linear path. Thanks to this process, larger and more complex geometries can be welded together. Consequently, this feature makes LFW applicable for complex designs and/or components with significant dimensional differences. In addition, precise control of welding parameters in LFW enables the production of joints with minimal distortion and results in superior mechanical performance [7–10]. Another notable type of friction welding is Rotary Friction Welding (RFW), in which one workpiece rotates against a stationary component. RFW is a very suitable method for combining materials with different cross-sectional areas. It is particularly suitable for welding high-strength joints in materials with cylindrical or tubular geometry. This method is widely adopted for applications in the automotive and aerospace industries, where dissimilar materials, for instance, steel, superalloys, and aluminum alloys, need to be joined effectively [10–13]. The main disadvantages of RFW are the high device cost and the axial shortening of the materials during the welding process [14, 15]. Another friction welding method is Friction Stir Welding (FSW), which represents a distinct approach that involves the rotation of a non-consumable tool, such as a pin or a rod, within the joint interface. This movement generates frictional heat, plasticizing the material surrounding the tool and, upon extraction, forming a bond. FSW has proven to be a reliable technique, especially for joining materials that are difficult to weld and require high strength [16]. This method is suitable even for light alloys used in the automotive and marine sectors [17–22].

Nickel-based superalloys are well known for their exceptional corrosion resistance, superior creep behavior, and higher tensile strength properties at high temperatures. Thanks to these properties, they are widely used in applications such as jet engines, power plants, and marine diesel engine components [23]. Inconel 718 alloy is one of the eminent nickel-based superalloys. It can be hardened only by precipitation hardening. It also exhibits excellent weldability due to its inherent resistance to strain-aging cracking. The favorable weldability properties of Inconel 718 are linked to the precipitation kinetics of the Ni_3Nb , γ'' -phase. However, these alloys have limited application areas. The main reason for that is their high costs. To reduce costs, alternative materials can be considered in place of Inconel 718 when less severe service conditions are encountered [24–26]. Generally, during conventional welding of Inconel 718 superalloy, the formation of laves phases, niobium or boron segregation, and liquation cracking may occur [26]. Friction welding is a well-known SSW technique capable of minimizing such

problems [27, 28].

AISI 316L is a widely used austenitic stainless steel in industry. It is preferred due to its exceptional corrosion resistance, formability, ductility, and toughness properties. These cost-effective structural materials find extensive applications in a variety of industries such as cryogenic vessels, cutlery, housewares, cookware, medical equipment, automotive, and aerospace structures, where they are manufactured into different components [29, 30]. Regarded as the most weldable stainless-steel type, austenitic stainless steel is frequently joined by fusion or resistance welding. Nevertheless, these welding techniques can lead to sensitization in the HAZ and facilitate the occurrence of solidification cracking or hot cracking. The sensitization phenomenon results in the formation and precipitation of chromium carbide at grain boundaries, particularly where carbon is abundant. As a result of these fusion and resistance welding processes, corrosion resistance decreases due to reduced chromium content in the affected area [31, 32]. To minimize these problems as much as possible, low-carbon AISI 316L stainless steel can be selected, as its low carbon content further reduces chromium carbide formation.

In reviewing the literature on the welding of Inconel 718 and AISI 316L, several studies were identified. The friction welding technique was applied to Inconel 718 superalloy with a different weldable material [33–39]. In addition, Gas Tungsten Arc Welding (GTAW), Electron Beam Welding (EBM), and Laser Welding (LW) methods were used to weld Inconel 718 superalloy to dissimilar materials [40]. Among them, D. K. Ramkumar et al. used Pulse Current Gas Tungsten Arc Welding (PCGTAW) and Continuous Current Gas Tungsten Arc Welding (CCGTAW) methods [41]. In their study, they used ER2553 and ErNiCu-7 as filling materials. Following SEM examinations of the welded specimens, they observed that there was an unmixed region in the HAZ of Inconel 718 for all welded specimens. They also stated that undesirable phases did not form in welds with ErNiCu-7 as the filler material. According to the tensile test results of the welded specimens, the ruptures occurred in the AISI 316L base material. Moreover, they concluded that better metallurgical and mechanical properties were obtained with the PCGTAW welding method using ErNiCu-7 as the filler material [41]. In another study, Y. F. Li et al. welded these two different alloys using the Electrically Assisted Pressure Joining (EAPJ) method, achieving crack- and gap-free welds. As a consequence of the tensile tests on the welded parts, they found that the ruptures occurred on the SUS 316L material side as it behaves more ductilely. They presented that these two dissimilar materials can be welded seamlessly by this SSW method [42]. Bansal A. et al. used the Microwave Welding method to weld these materials. They performed the weld-

Table 1. Percentage weight of Inconel 718 and AISI 316L

Elements	Al	B	C	Co	Cr	Cu	Fe	Mn	Mo	Nb	Ni	P	S	Si	Ti
Inconel 718	0.48	0.004	0.03	0.26	19.3	0.05	17.5	0.07	3.02	5.23	53.0	0.007	0.001	0.05	0.96
AISI 316L	–	–	0.017	–	16.576	0.356	Bal.	1.308	2.031	–	10.128	0.0315	0.0254	0.42	–

ing process by adding Inconel 718 powder between the surfaces to be welded. They measured an average hardness of 230 ± 5 HV at the weld interface. In addition, they conducted tensile tests on the welded specimens. Consequently, they stated that the ruptures occurred in the weld zone. Also, the measured tensile strengths were lower than the tensile strength of the AISI 316L base material [43]. Hinojos A. et al. repeated the welding process using powders of these two different materials with the Electron Beam Melting (EBM) method. In the method they used, a piece was first printed from Inconel 718 powder. Later, a single piece was obtained by printing with AISI 316L powders. SEM, EDS, and XRD analyses of welded specimens showed that the NbC content increased and the melting point decreased. Thus, they concluded that the EBM method can be used alongside traditional welding methods [44]. Lalam S. V. et al. used the CDFW technique to weld dissimilar materials, including EN24 and Inconel 718. The welding process involved specific parameters, such as a friction pressure of 28 kN, a forge pressure of 41.73 kN, a rotational speed of 1422 rpm, and a burn-off length of 5 mm. After welding, the welded parts underwent two distinct heat-treatment processes. In their studies, they compared the microstructural and mechanical properties of the welded specimens produced using the specified parameters. The results showed that friction welding of these dissimilar metals exhibited superior toughness but lower strength than their base metals. The toughness value decreased after the first heat treatment; conversely, the tensile strength increased. There was a moderate improvement in strength but a significant reduction in toughness after the second heat treatment [45]. Beeravolu A. R. et al. used the RFW method to Inconel 718 to AISI 316L. They subjected Inconel 718 to two different heat treatments before welding. Some of the friction-welded specimens were subjected to direct post-weld ageing treatment (PWHT). They evaluated the mechanical, grain size, and microstructural properties of welded specimens. They found that, due to compression and softening of the weld zone at high rotational speeds, an intermixed zone formed at the weld interface. Of the welded specimens, the PWHT specimens showed high strength. This could be related to the formation of precipitates. In addition, with the formation of precipitates in the Fully Deformed Zone (FDZ), the highest hardness values were acquired in PWHT welded specimens compared to other welding conditions [33].

In this paper, a superalloy (Inconel 718) and an austenitic stainless steel (AISI 316L) were welded using the CDFW method, a frequently preferred friction welding technique. The main parameters affecting the welding quality in CDFW are rotational speed (rpm), friction time (s), friction pressure (MPa), forge time (s), and forge pressure (MPa) [3, 46, 47]. Although there are many studies in the literature on the friction welding of superalloys and stainless steels separately, there are only a few that report on dissimilar friction welding of Inconel 718 and AISI 316L. The main objective of the present study is to evaluate the impact of CDFW parameters. In this context, three main parameters and three levels for each parameter were determined based on the literature. Thus, 27 combinations were created in total. The other original aim of this study is to determine the optimum combination based on mechanical properties as a result of experimental studies for the determined combinations. Furthermore, it aims to analyze the microstructural and macrostructural changes after the CDFW process. Finally, the mechanical properties of the welded specimens were examined using hardness and tensile tests. According to the literature, it is clear that to achieve higher mechanical properties in welded dissimilar materials, some pre- or post-heat treatment processes are needed. One of the non-ignorable outcomes of this study is that, thanks to the determined welding parameter combination, these mechanical property performances for welded Inconel 718 and AISI 316L materials were achieved without any pre- or post-heat treatment.

2. Materials and methods

In this study, Inconel 718 and AISI 316L were selected for welding using the CDFW method. The chemical composition of Inconel 718 and AISI 316L materials is given in Table 1, and their mechanical and thermal properties are given in Table 2. The specimens were prepared with a diameter of 12 mm and a length of 70 mm for welding. Before welding, since the cutting marks on the specimens' surfaces were relatively deep, all specimens to be welded underwent polishing. The surfaces of all specimens were polished with 80-, 600-, and 1200-mesh SiC abrasive sandpapers and with broadcloth, respectively. Finally, all of the polished specimens were cleaned with an ultrasonic cleaner in 50 % C_3H_6O (acetone) solution.

Table 2. Mechanical and thermal properties of Inconel 718 and AISI 316L

Material	UTS (MPa)	Elongation at break (%)	Vickers hardness HV10	Thermal conductivity ($\text{W m}^{-1}\text{K}^{-1}$)
Inconel 718	939.1	48.13	235	11.4
AISI 316L	772.6	51.43	229	14.0 – 15.9

Table 3. CDFW parameters [14]

Specimens	Specified parameters				
	Rotation speed (rpm)	Friction time (s)	Friction pressure (MPa)	Forge pressure (MPa)	Forge time (s)
S1	1800	16	60	120	32
S2			40	80	
S3			20	40	
S4	1800	12	60	120	24
S5			40	80	
S6			20	40	
S7	1600	6	60	120	12
S8			40	80	
S9			20	40	
S10	1600	16	60	120	32
S11			40	80	
S12			20	40	
S13	1600	12	60	120	24
S14			40	80	
S15			20	40	
S16	1400	6	60	120	12
S17			40	80	
S18			20	40	
S19	1400	16	60	120	32
S20			40	80	
S21			20	40	
S22	1400	12	60	120	24
S23			40	80	
S24			20	40	
S25	1400	6	60	120	12
S26			40	80	
S27			20	40	

A total of 27 different welding parameter combinations were used for CDFW. Basically, three different speeds, three different friction times, and three different friction pressures were determined. The determined welding parameters are listed in Table 3.

The experimental setup of CDFW is illustrated in Fig. 1. In experiments, the Inconel 718 specimen was fixed to the chuck providing linear motion, as indicated by the orange arrow, and the AISI 316L specimen was fixed to the chuck providing linear motion, as indicated by the red arrow, and the AISI 316L specimen was fixed to the chuck with rotational movement,

as shown with the blue splined arrow. The CDFW process was performed using hydraulically operated CDFW equipment specifically designed for this purpose [48]. According to the specified parameters, a total of 108 specimens were welded using this setup for mechanical testing and microstructural analysis. One of the welded specimens is illustrated in Fig. 2a for the S1 case specimen.

After the CDFW process, the specimens were sectioned along the transverse axis for microstructure and hardness analyses (Fig. 2b). The surfaces to be analyzed were polished with sandpaper up to 2000 grit.

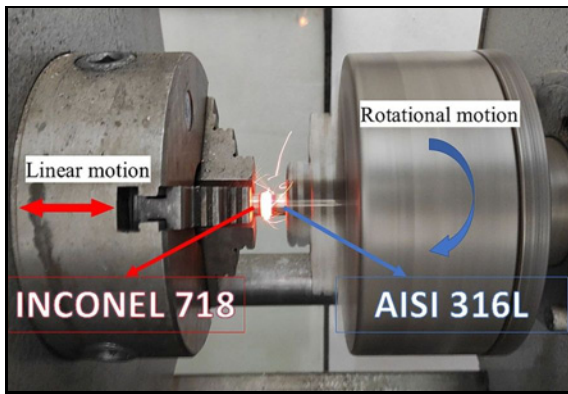


Fig. 1. CDFW application image.

To examine the microstructure of the welded specimens more clearly, the specimens were etched. For the Inconel 718 side, a solution of 85 ml distilled water (H₂O), 5 ml glacial acetic acid, and 10 ml HNO₃ was prepared as an etchant [45]. It was electrolytically etched with this solution for 3 s at 2 V. After etching Inconel 718, a second etchant solution was applied to AISI 316L material containing 30 ml distilled water, 20 ml HCl, and 10 ml HNO₃, and was applied for 50 seconds [49].

Hardness tests were performed according to ASTM E92-17, Standard Test Methods for Vickers Hardness and Knoop Hardness of Metallic Materials [50]. The test parameters were a 10 kg load with an 11-second dwell time. The measurements were obtained at 21 points with 1 mm spacing, as shown in Fig. 2c, using the Mitutoyo KK810-165D Vickers Hardness Tester for each welded specimen.

In terms of tensile tests, welded specimens were machined according to the dimensions as given in Fig. 3 in accordance with ASTM E8/E8M tensile standards [51]. The tests were conducted under a 250 kN load capacity at a crosshead speed of 2 mm min⁻¹, with 31 % humidity and an ambient temperature of 18°C, using a SHIMADZU AG-X model testing machine.

3. Results and discussion

3.1. Macrostructure of the welded specimens

Inconel 718 and AISI 316L specimens were welded using 27 different welding parameter combinations. As an example of these welded specimens, macro photographs of S1, S4, and S7 specimens welded at 1800 rpm are presented in Fig. 4. As illustrated in Fig. 4, the weld joints exhibit good flashes at 16 s and 12 s friction time. During this period, as a result of frictional forces sufficient heat was generated to plasticize the materials at the interface [33]. At 6 s friction time,

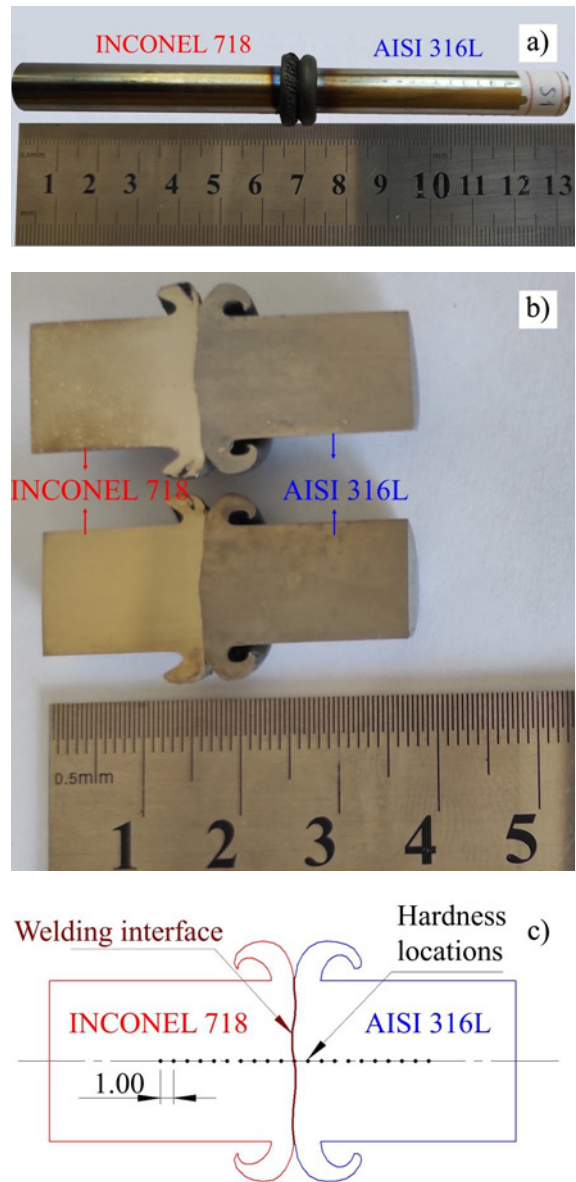


Fig. 2. (a) Welded specimen: (b) cross section and (c) hardness measurement locations.

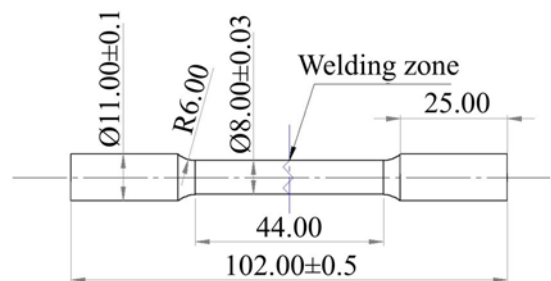


Fig. 3. Tensile test specimen dimensions.

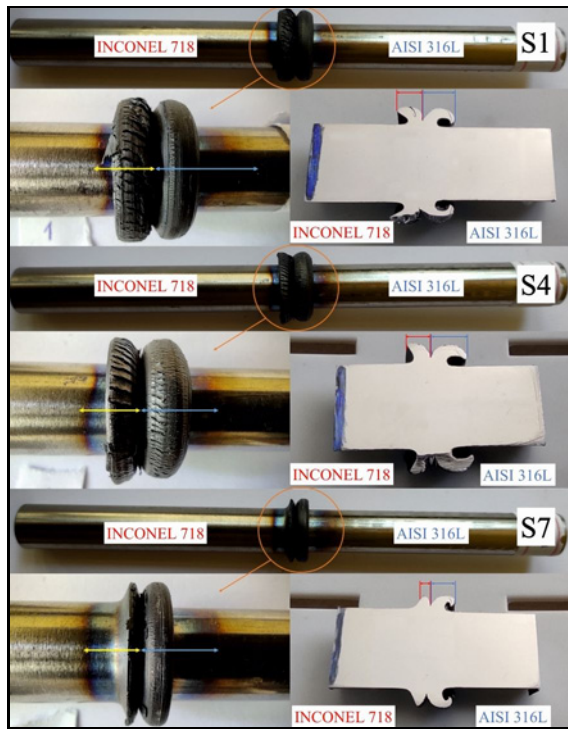
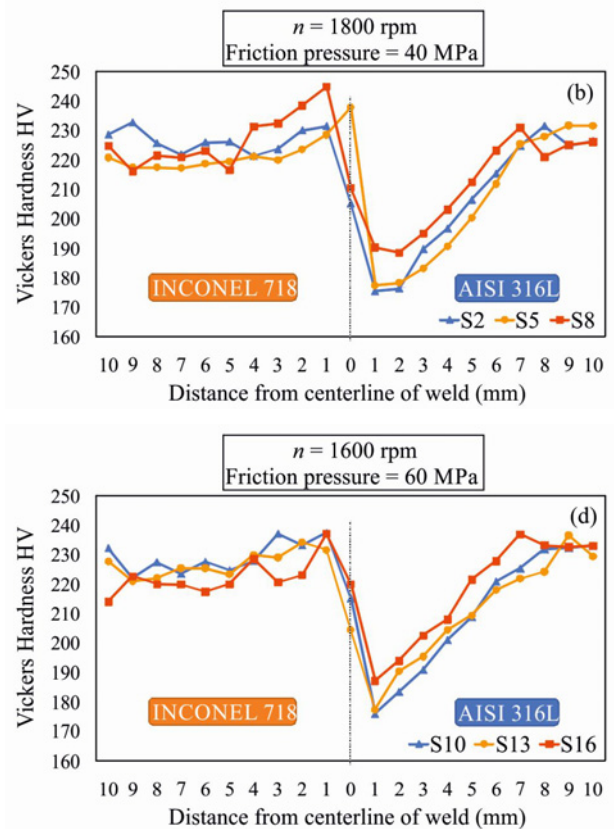
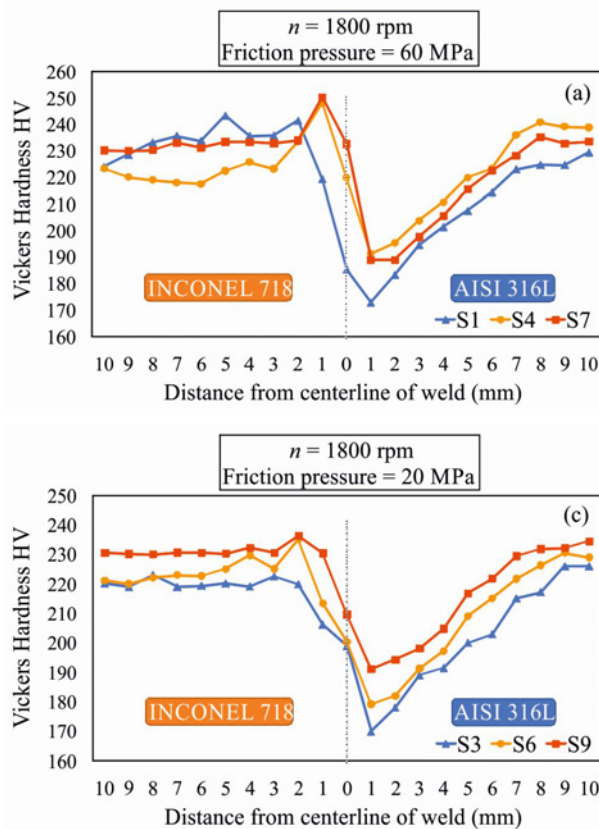


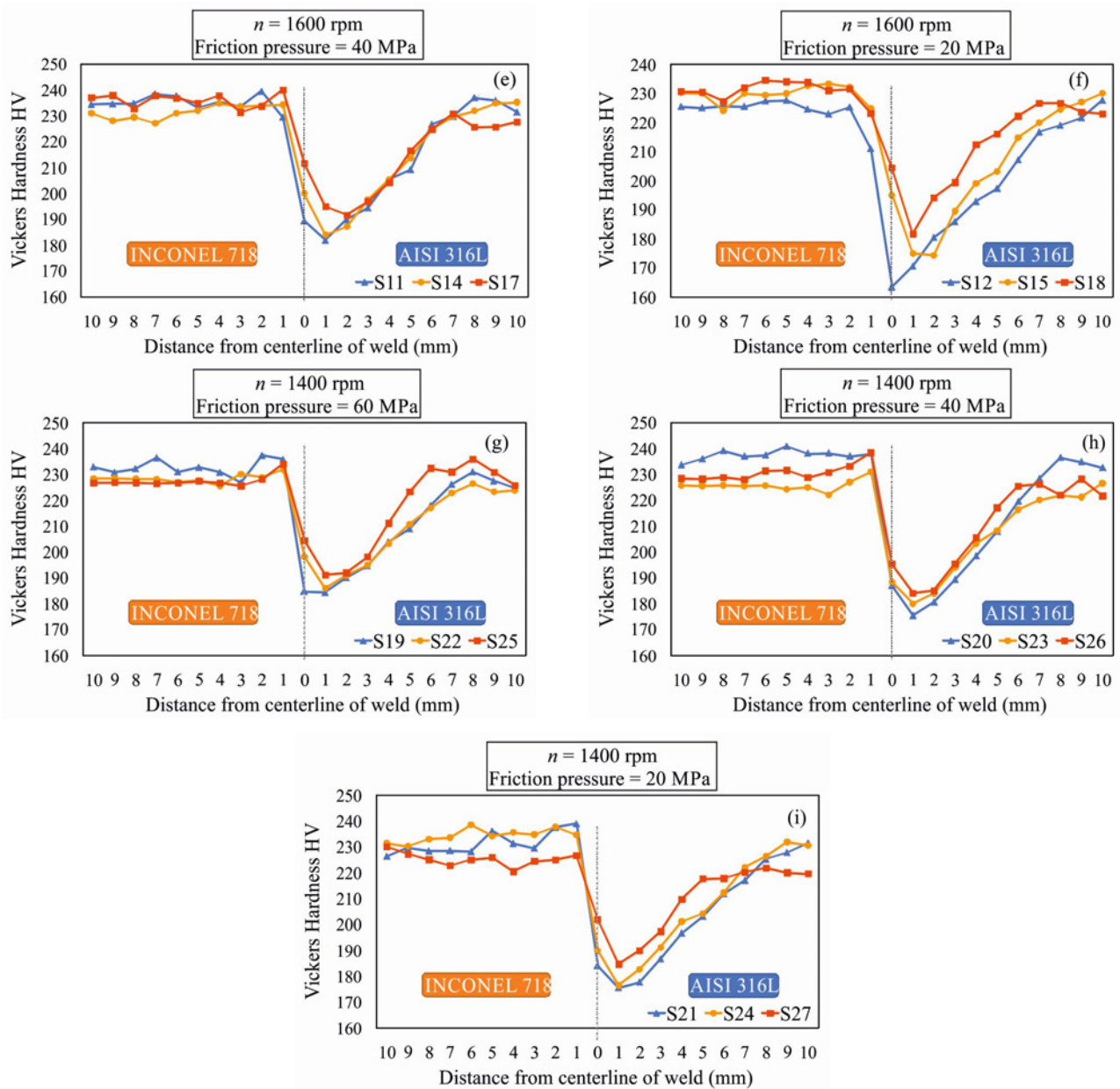
Fig. 4. Macro photographs of S1, S4, and S7.

flash was insufficiently formed on the side of Inconel 718 material. Typical friction welding flash shape did not occur [52]. This shows that the welding parameter combinations made at 1800 rpm rotation speed and 6 s friction time are insufficient for these two dissimilar materials. During the examination of the welding flashes, cracks have been observed on the Inconel 718 material side. These cracks can be attributed to the higher hardness of Inconel 718 compared to AISI 316L at elevated temperatures during welding. Similarly, N. Y. Kim et al. came to the same conclusion in their studies [38]. The dominance of flash generation was also observed on the AISI 316L side compared to the Inconel 718 side. This difference in flash formation can be attributed to the higher strength of Inconel 718 at elevated temperatures than AISI 316L during the friction welding process. In contrast, AISI 316L experiences a significant reduction in flow stress at higher temperatures, causing the alloy to soften and undergo plastic deformation more easily [33, 34, 38].

The different rates of color change in Inconel 718 and AISI 316L materials within the weld zone can also be evaluated. On the Inconel 718 side, indicated by the yellow arrow, the color change appears distinct and sharp, concentrated within a narrow region. This can be attributed to the more intense heat accumulation



Figs. 5a–d. Vickers hardness variation graphs for welded specimens.



Figs. 5e–i. Vickers hardness variation graphs for welded specimens.

on the surface, resulting from the low thermal conductivity and high-temperature resistance of Inconel 718. In contrast, on the AISI 316L side, indicated by the blue arrow, the color transition is smoother and occurs over a wider area. This is due to the higher thermal conductivity of AISI 316L compared to Inconel 718. It is clearly observed that as the heat input increases with longer friction times, the extent of color change in both materials becomes even wider.

3.2. Mechanical properties

A total of 577 hardness measurements were taken from 27 different welded specimens, including Inconel

718 and AISI 316L base materials. Since the hardness parameters were numerous, hardness changes in the weld zone were grouped by welds at the same rotation speed and friction pressure. Thus, three welded specimens were compared based on the variation in friction time in each graph. Hardness analysis graphs are shown in Figs. 5a–i.

The hardness of the base materials was measured at 235 HV10 for the Inconel 718 specimen and 229 HV10 for the AISI 316L specimen. According to the hardness analysis, the AISI 316L material showed a decrease in hardness in the weld zone. Austenitic stainless steels, especially AISI 316L, undergo significant microstructural changes at elevated tempera-

tures due to their low carbon content and high nickel-chromium ratio. The thermomechanical effects during friction welding activates grain growth and stress-relief mechanisms, especially in the weld center. This results in a significant decrease in the material's hardness. In addition, since AISI 316L has a face-centered cubic (FCC) structure, grain boundary migration and dislocation movement are more readily observed at high temperatures. As grain growth increases under high-temperature conditions, the material's hardness decreases [53]. This is shown in Figs. 11a,b in the microstructure analysis section.

On the Inconel 718 side, hardness appears to be more stable and is generally higher than that of AISI 316L. All graphs show a significant decrease in hardness at the weld center. This may be due to softening of the microstructure caused by the thermal effect of friction welding. Inconel 718, on the other hand, due to its niobium and molybdenum content, suppresses grain boundary movement at high temperatures and becomes more resistant to hardness loss. This explains the ability of the Inconel side to maintain higher hardness values in the friction-welded region [54].

At 1800 rpm, the hardness values show a sharp drop in the weld center, while at lower speeds (1400 rpm), this drop is less pronounced. When higher friction pressure (60 MPa) is applied, the hardness drop in the weld zone is generally less pronounced. This may be because higher pressure increases material flow, resulting in better metallurgical bonding. For welds with a lower friction pressure (20 MPa), the hardness drop is sharper and decreases to lower values in the center [55].

Tensile tests were performed on the welded specimens, and the UTS of the Inconel 718 specimen was found to be 939 MPa, and the UTS of the AISI 316L material was found to be 772.6 MPa. In tensile tests, all specimens ruptured in the HAZ of the AISI 316L material side. For instance, the tensile test rupture surfaces of specimens S2, S5, and S8 welded with the main parameters of 1800 rpm and 40 MPa friction pressure are shown in Fig. 6.

Cross-sectional narrowing, dimples, and roughness on the surfaces of the ruptured specimens indicate that the ductile rupture mechanism is dominant. The rupture mechanism is also discussed in detail in the microstructure evaluation section. Stress-strain graphs for specimens S2, S5, and S8, which are given in Fig. 6 as a result of tensile tests, are given in Fig. 7.

To compare the UTS of the base Inconel 718 material, the base AISI 316L material, and 27 different welded specimens, a bar graph was created, as shown in Fig. 8. When the UTSs of the welded specimens are compared, although the welding parameters of all specimens differ, the maximum UTS was measured at 736.3 MPa in the welded S17 specimen with a rotational speed of 1600 rpm, a friction time of 6 s, and a



Fig. 6. S2, S5, and S8 tensile specimens and rupture surfaces.

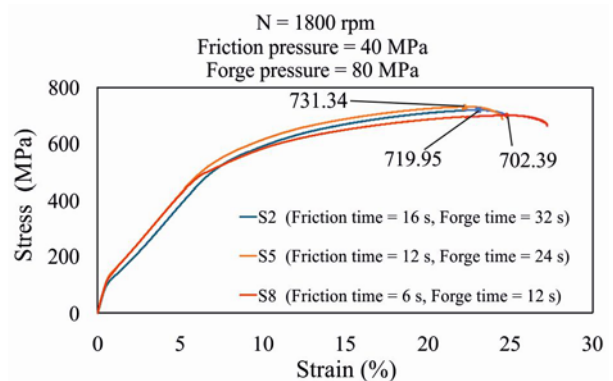


Fig. 7. Stress-strain tensile graphs of specimens S2, S5, and S8.

friction pressure of 40 MPa. The minimum UTS was measured as 653.6 MPa for the S24 specimen when the rotational speed was 1400 rpm, the friction time was 12 s, and the friction pressure was 20 MPa. Friction-welding studies for these two materials were carried out after heat treatment, as reported in the literature. Beeravolu, A. R. et al. reported a maximum tensile strength of 728 MPa in their study [33]. In this study, it was observed that better mechanical properties were obtained with the welding parameters determined without any heat treatment. Thanks to this enhancement, it is believed to contribute to the literature and to apply to researchers and industrial areas.

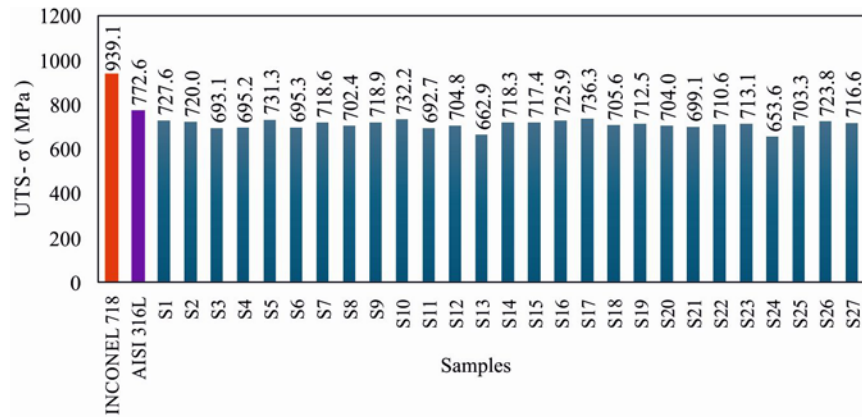


Fig. 8. Ultimate tensile strength (UTS) of specimens.

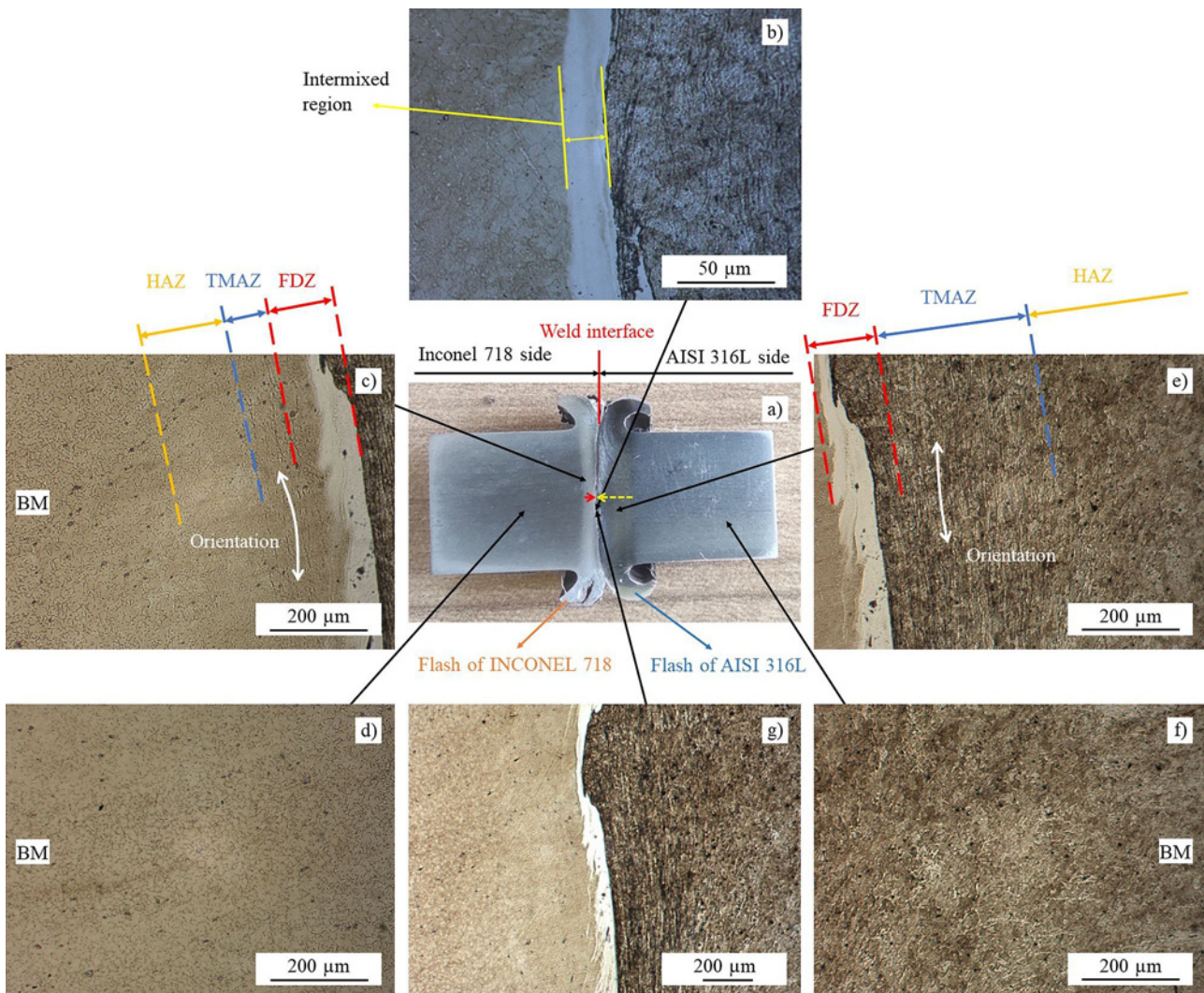


Fig. 9. Optical microscope images of S4 (a) cross-section of specimen, (b) 400× magnification of weld interface, (c) welding regions of Inconel 718, (d) 100× magnification of Inconel 718 base metal, (e) welding regions of AISI 316L, (f) 100× magnification of AISI 316L, and (g) 100× magnification of weld interface.

3.3. Microstructure properties

In friction welding, the weld cross-section contains

distinctive regions. These regions are called Fully Deformed Zone (FDZ), Thermo-Mechanically Affected Zone (TMAZ), HAZ- and Base Metal (BM). Opti-

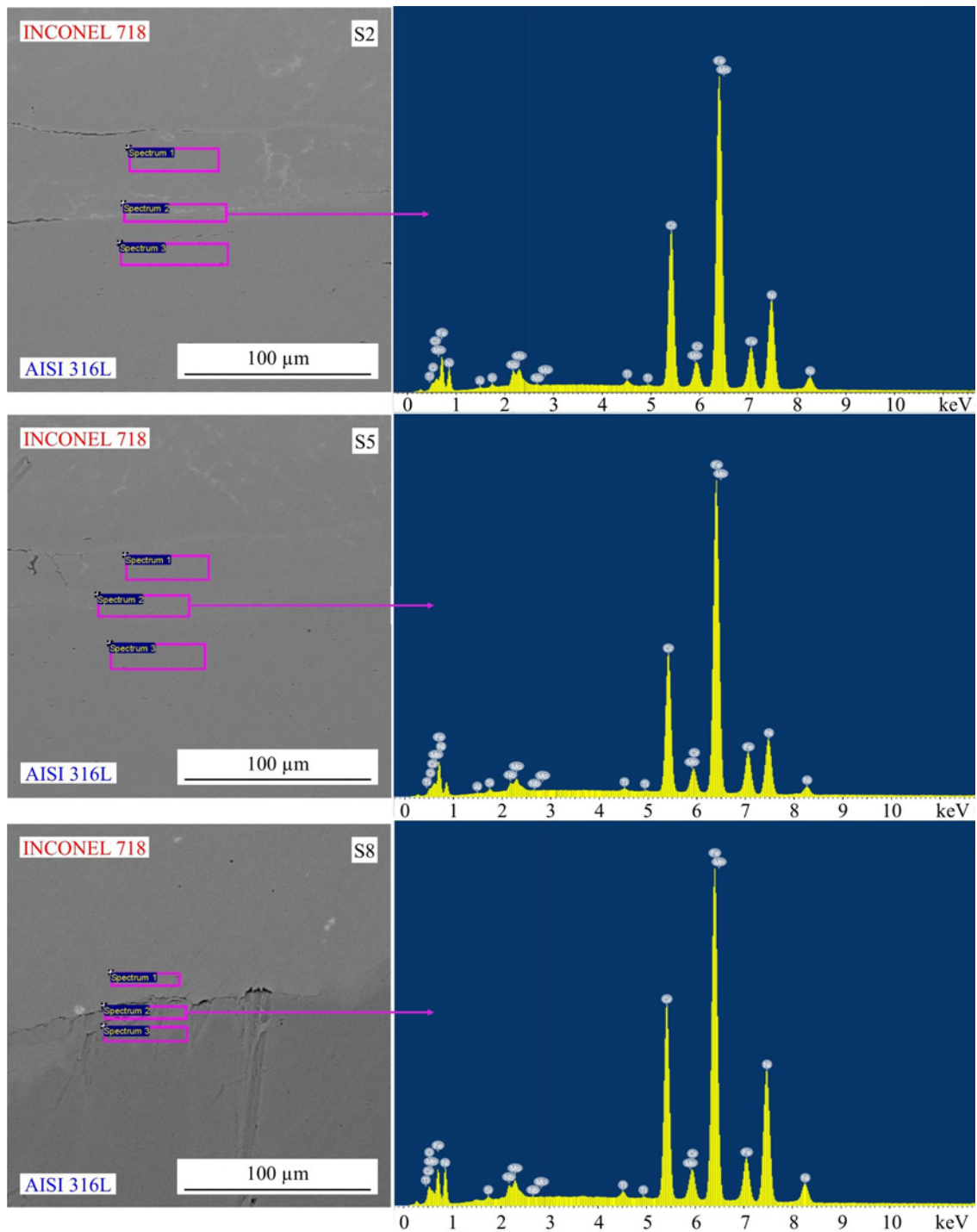


Fig. 10. SEM and EDS images of S2, S5, and S8.

cal Microscope images and weld zones of S4 specimen welded with 1800 rpm rotation speed, 12 s friction time and 60 MPa friction pressure welding parameters are shown in Fig. 9. The etched specimen is given in Fig. 9a. Upon examination, it can be seen that the area affected by welding on the Inconel 718 side (indicated by the dashed red arrow) is narrower than that on the AISI 316L side (indicated by the dashed yellow arrow). In the optical microscope images given in

Figs. 9b and 9g, the intermixed zone in the weld region is observed. The intermixed region is the zone where the two materials are completely mixed and lies within the FDZ. EDS analysis of this region revealed distinct variations in the ratios of Ni, Cr, and Fe [34, 39]. This is also an indication of the intermixed zone (Fig. 10). The intermixed zone was observed in all welds. FDZ, TMAZ, and HAZ regions are shown in Figs. 9c and 9e for Inconel 718 and AISI 316L, respectively. The

Table 4. EDS analysis of S2, S5, and S8

Specimen	Spectrum	Elements (wt.%)						
		Cr	Fe	Nb	Ni	Mn	Mo	Si
S2	1	17.83	60.2	1.26	16.19	1.38	2.39	0.53
	2	17.40	50.04	4.08	21.82	1.12	3.03	0.42
	3	17.60	67.74	–	10.09	1.58	2.46	0.53
S5	1	17.83	60.87	1.29	15.46	1.41	2.47	0.50
	2	17.36	57.82	2.41	16.00	1.40	2.64	0.52
	3	17.86	68.14	–	9.69	1.49	2.30	0.53
S8	1	20.16	17.54	4.52	50.12	0.24	3.05	0.24
	2	18.06	43.89	2.66	26.71	0.93	2.75	0.41
	3	17.98	60.30	–	16.21	1.31	2.18	0.49

white arrows also show the grain orientations resulting from friction welding in these two dissimilar materials. FDZ, TMAZ, and HAZ in Inconel 718 are narrower than those in AISI 316L. This is evident from the color change in the weld area in the macro photographs in Fig. 4, indicated by the yellow and blue arrows. Figures 9d and 9f show the internal structure of the weld unaffected zone, i.e., the base metal, of Inconel 718 and AISI 316L materials, respectively.

SEM and EDS analyses of the weld interface sections of the welded specimens were performed. After the analysis, no cracks or gaps were observed in the weld area. The weld zones along the weld line were also examined under an optical microscope, and it was observed that the joint was complete. SEM and EDS images of S2, S5, and S8 specimens welded with 1800 rpm rotational speed and 40 MPa friction pressure parameters are shown in Fig. 10, and EDS analysis data are shown in Table 4. EDS analyses were evaluated according to the weight % of Fe, Ni, and Nb elements in the selected regions in Fig. 10. According to the Spectrum 3 EDS data, it is seen that there is no Nb element in S2, S5, and S8 specimens, and therefore, this region is on the side of AISI 316L material. The low Ni ratio in the Spectrum 1 and 2 EDS data, and the presence of the Nb element in these regions, confirm that these zones are intermixture regions. However, as seen in the Spectrum 1 EDS analysis of specimen S8, the selected region is Inconel 718 material [39].

The tensile test results showed that the welded specimens ruptured on the AISI 316L side. In addition, hardness measurements revealed a decrease in hardness on the AISI 316L side. When the reason for the rupture from this side and the hardness decrease was investigated with an optical microscope, it was observed that there was grain growth in the AISI 316L material in the S21 specimen, as shown in Fig. 11b. The ruptures occurred in the HAZ where this grain growth occurred [56, 57]. As seen in Fig. 9c and 9e, TMAZ and HAZ are wider on the AISI 316L side than

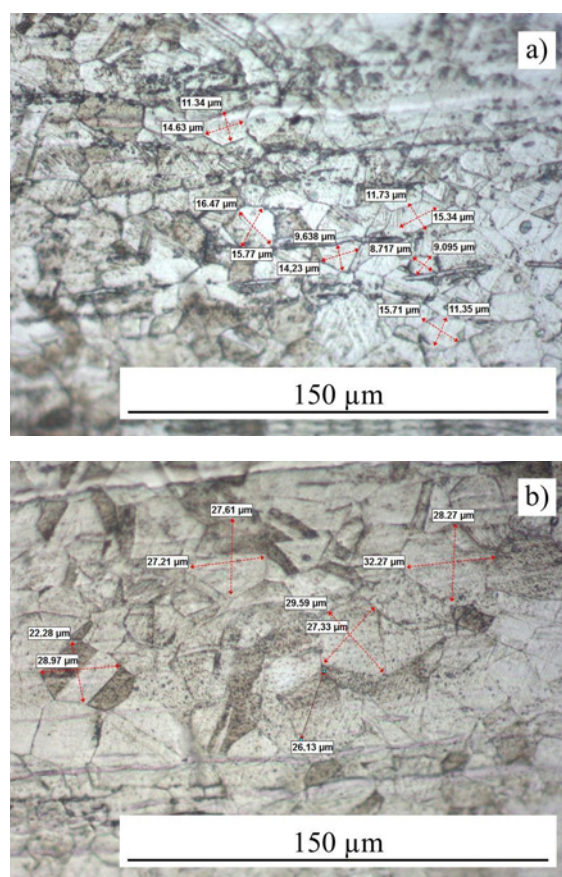


Fig. 11. (a) AISI 316L base material grain size and (b) AISI 316L HAZ grain size of S21 specimen.

on the Inconel 718 side. The hardness graphs show that the hardness of AISI 316L changes at a distance of 7–8 mm from the welding center, confirming this. On the Inconel 718 side, the TMAZ and HAZ are very narrow. It is approximately 0–2 mm away from the welding center. The effect of welding parameter combinations on hardness varied across welded specimens. When specimens with different rotational speeds and

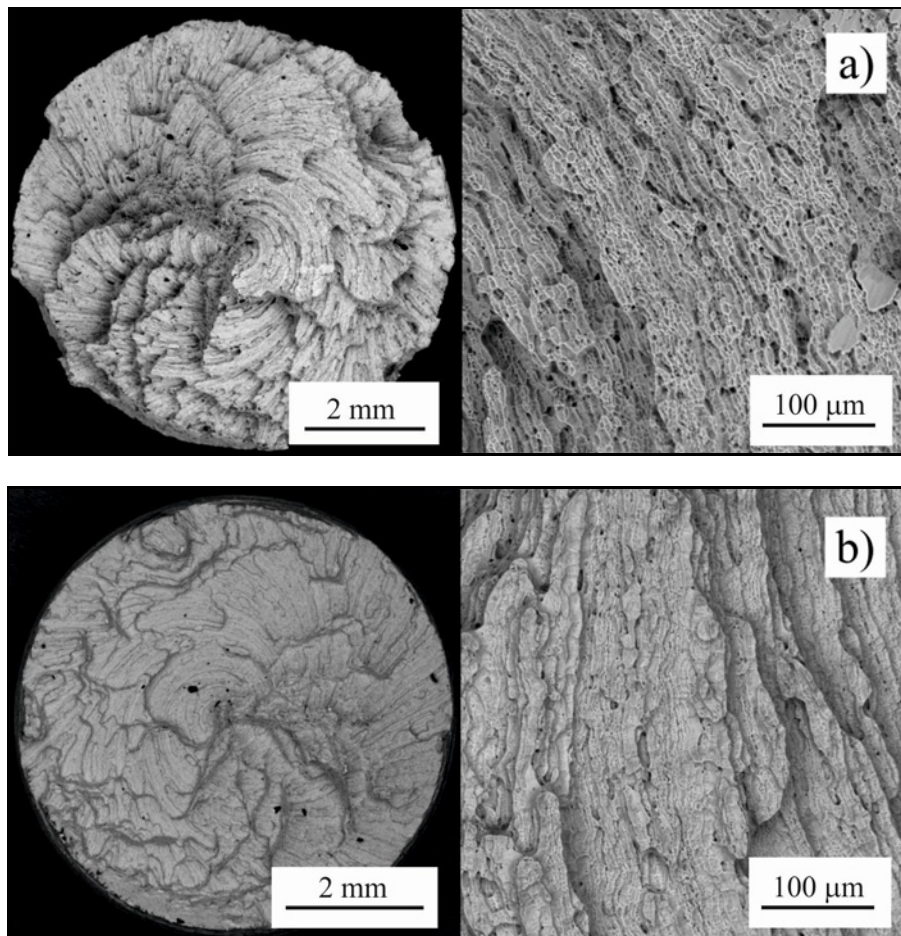


Fig. 12. (a) SEM image of the S2 specimen ruptured from the AISI 316L part and (b) SEM image of the S2 specimen ruptured from the INCONEL 718 part.

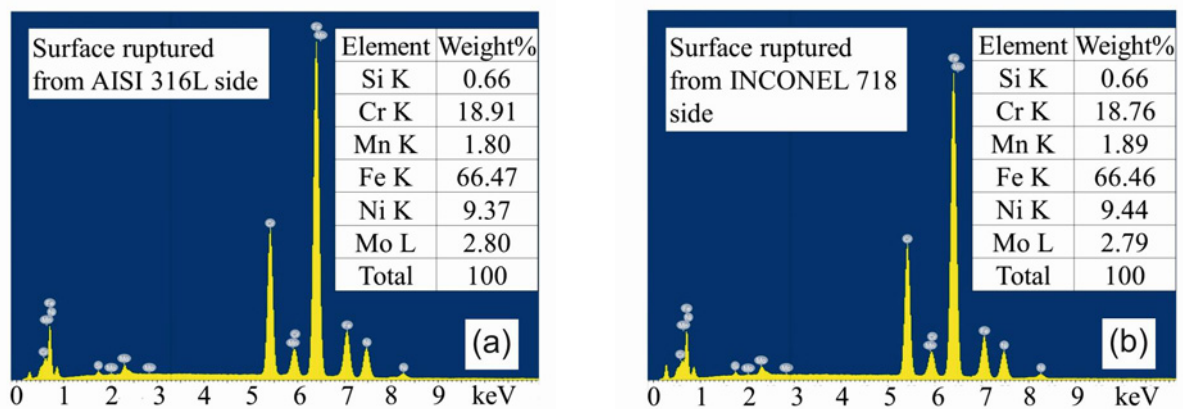


Fig. 13. EDS analysis of ruptured surfaces of S2 specimen: (a) AISI 316L and (b) INCONEL 718.

constant other welding parameters are compared, it is observed that the TMAZ and HAZ are wider at higher rotational speeds. The reason is that the heat input increases with higher rotational speed. At the same time, the TMAZ and HAZ are wider as the increase in friction pressure increases the heat input by increasing the friction pressure.

All ruptures resulting from tensile tests were evaluated through visual inspection on the AISI 316L side. SEM images and EDS analyses were performed on the ruptured specimens by selecting the images closest to the weld interface. These analyses were performed for specimens S1, S2, S3, S10, and S19. As an example, SEM images of specimen S2 are shown in Figs. 12a,b,

and EDS graphs are shown in Fig. 13.

The SEM images in Figs. 12a,b show that because of plastic deformation, crater-like dimples were formed perpendicular to the tensile direction. It is observed that the micro dimples coalesce to form larger dimples. This shows that cracks merge under tensile load and that this initiates rupture. In addition, there is no obvious grain boundary rupture or planar crack propagation in the images. These observations collectively confirm that the rupture mechanism is ductile. The presence of this dimpled structure indicates that plastic deformation is at a high level and rupture occurs by a micro-void coalescence mechanism [58, 59].

The EDS graphs and elemental ratios in Figs. 13a,b clearly show that the Cr content is approximately 18.5 wt%, the Ni content is around 9 wt.%, and the absence of Nb confirms that the cracking occurred entirely within the AISI 316L material.

4. Conclusions and recommendations

In this paper, Inconel 718 and AISI 316L were successfully welded by the CDFW method. The effects of different welding parameters on the quality of the welded joints were systematically investigated. The effect of predetermined welding parameters on the mechanical and microstructural properties of the welded specimens was investigated. The following conclusions were drawn:

1. For all welding parameter combinations, the dissimilar weld INC 718/AISI 316L was obtained without any cracks or incomplete joints. In addition, by examining the % element ratios by weight in the joints using EDS analyses, it was observed that complete mixing occurred.

2. The macrostructure of the welded specimens exhibited a greater occurrence of flash on the AISI 316L side compared to the Inconel 718 side. This indicates that the AISI 316L material underwent greater plastic deformation during the CDFW process.

3. As a result of macroscopic examinations, increasing the friction time, friction pressure, and rotational speed in the welded specimens led to an increase in HAZ width and weld flash size.

4. When the hardness distributions were examined, no significant hardness change was observed in Inconel 718 material, and a decrease in hardness was observed in AISI 316L material. Grain coarsening was observed in the regions where this hardness decrease occurred. It is thought that this is due to slow cooling after welding, caused by the low thermal conductivity of AISI 316L. In addition, this hardness decrease can be prevented by controlling the cooling rate after welding under control.

5. The tensile specimens ruptured in the HAZ region on the AISI 316L side for all of the dissimilar

welded specimens. This results from the HAZ having grains larger than those of both the weld interface and the parent metal.

6. Friction welding of dissimilar INC 718/AISI316L materials was found to have slightly lower UTS than non-welded specimens. The maximum UTS was obtained as 736.3 MPa in specimen S17 at 1600 rpm, 6 s friction time, and 40 MPa friction pressure parameters.

In conclusion, it has been shown that these two dissimilar materials can be successfully joined by the CDFW method. Furthermore, thanks to these optimized welding parameters, higher mechanical and microstructural property enhancements were achieved without the need for additional pre- or post-processes, such as heat treatment before welding. Consequently, this achievement simplifies the application and reduces processing time. Accordingly, the cost of production will also be reduced due to the advantages of this study.

Acknowledgement

This work is supported by the Scientific Research Project Fund of Sivas Cumhuriyet University under the project number M-789.

References

- [1] J. F. Lancaster, Metallurgy of Welding, 6th ed., Abington Publishing, 1999.
- [2] M. B. Uday, M. N. Ahmad Fauzi, H. Zuhailawati, A. B. Ismail, Advances in friction welding process: A review, Sci. Technol. Weld. Join. 15 (2010) 534–558. <https://doi.org/10.1179/136217110X12785889550064>
- [3] W. Li, A. Vairis, M. Preuss, T. Ma, Linear and rotary friction welding review, Int. Mater. Rev. 61 (2016) 71–100. <https://doi.org/10.1080/09506608.2015.1109214>
- [4] E. D. Nicholas, Friction processing technologies, Weld. World 47 (2003) 2–9. <https://doi.org/10.1007/BF03266402>
- [5] M. Aritoshi, K. Okita, Friction welding of dissimilar metals, Weld. Int. 17 (2003) 271–275. <https://doi.org/10.1533/wint.2003.3112>
- [6] M. Maalekian, Friction welding – critical assessment of literature, Sci. Technol. Weld. Join. 12 (2007) 738–759. <https://doi.org/10.1179/174329307X249333>
- [7] A. Chamanfar, M. Jahazi, J. Cormier, A Review on inertia and linear friction welding of Ni-based superalloys, Metall. Mater. Trans. A 46 (2015) 1639–1669. <https://doi.org/10.1007/s11661-015-2752-4>
- [8] A. Chamanfar, M. Jahazi, J. Gholipour, P. Wanjara, S. Yue, Mechanical property and microstructure of linear friction welded Waspaloy, Metall. Mater. Trans. A 42 (2011) 729–744. <https://doi.org/10.1007/s11661-010-0457-2>
- [9] T. Saju, M. Velu, Review on welding and fracture of nickel based superalloys, Mater. Today Proc. 46 (2021)

- 7161–7169.
<https://doi.org/10.1016/j.matpr.2020.11.334>
- [10] V. Ajay, N. K. Babu, M. Ashfaq, T. M. Kumar, K. V. Krishna, A review on rotary and linear friction welding of inconel alloys, *Trans. Indian Inst. Met.* 74 (2021) 2583–2598.
<https://doi.org/10.1007/s12666-021-02345-z>
- [11] W. M. Gan, M. Hofmann, V. Ventzke, C. Randau, Y. D. Huang, A. Kriele, H. G. Brokmeier, M. Mueller, Microstructure and residual stress in rotary friction welded dissimilar metals of AA7020 aluminium alloy with 316L steel, *Mater. Sci. Forum* 879 (2017) 572–577. <https://doi.org/10.4028/www.scientific.net/MSF.879.572>
- [12] T. Saju, M. Velu, Characterization of welded joints of dissimilar nickel-based superalloys by electron beam and rotary friction welding, *J. Mater. Eng. Perform.* 31 (2022) 9462–9480.
<https://doi.org/10.1007/s11665-022-06958-3>
- [13] A. U. Rehman, N. Kishore Babu, M. K. Talari, S. Anwar, Y. Usmani, A. M. Al-Samhan, dissimilar rotary friction welding of Inconel 718 to F22 using Inconel 625 interlayer, *Appl. Sci.* 11 (2021) 10684.
<https://doi.org/10.3390/app112210684>
- [14] Ö. Karabey, A. Akkuş, Effect of welding parameters on axial shortening in continuous friction welded Inconel 718 superalloy and AISI 316L stainless steel, *Avrupa Bilim Ve Teknol. Derg.* (2022) 311–316.
<https://doi.org/10.31590/ejosat.1081747>
- [15] F. F. Wang, W. Y. Li, J. L. Li, A. Vairis, Process parameter analysis of inertia friction welding nickel-based superalloy, *Int. J. Adv. Manuf. Technol.* 71 (2014) 1909–1918.
<https://doi.org/10.1007/s00170-013-5569-6>
- [16] R. Kumar, V. Upadhyay, C. Pandey, Effect of post-weld heat treatments on microstructure and mechanical properties of friction stir welding joints of AA2014 and AA7075, *J. Mater. Eng. Perform.* 32 (2023) 10989–10999.
<https://doi.org/10.1007/s11665-023-07927-0>
- [17] D. Kumar Rajak, D. D. Pagar, P. L. Menezes, A. Eyvazian, Friction-based welding processes: friction welding and friction stir welding, *J. Adhes. Sci. Technol.* 34 (2020) 2613–2637.
<https://doi.org/10.1080/01694243.2020.1780716>
- [18] P. L. Threadgill, Terminology in friction stir welding, *Sci. Technol. Weld. Join.* 12 (2007) 357–360.
<https://doi.org/10.1179/174329307X197629>
- [19] J. Martin, S. Wei, Friction Stir Welding Technology for Marine Applications, in: R. S. Mishra, M. W. Mahoney, Y. Sato, Y. Hovanski (Eds.), *Frict. Stir Weld. Process. VIII*, Springer International Publishing, Cham, 2016, pp. 219–226.
https://doi.org/10.1007/978-3-319-48173-9_24
- [20] M. Haghshenas, A. P. Gerlich, Joining of automotive sheet materials by friction-based welding methods: A review, *Eng. Sci. Technol. Int. J.* 21 (2018) 130–148.
<https://doi.org/10.1016/j.jestch.2018.02.008>
- [21] E. T. Akinlabi, R. M. Mahamood, *Solid-State Welding: Friction and Friction Stir Welding Processes*, Springer International Publishing, Cham, 2020.
<https://doi.org/10.1007/978-3-030-37015-2>
- [22] M. Karimi Estahbanati, M. Movahedi, Metallurgical aspects and wear performance of Al/(Fe–Cu)_p hybrid composite produced using friction stir processing, *Met. Mater. Int.* 30 (2024) 284–302.
<https://doi.org/10.1007/s12540-023-01498-4>
- [23] O. Roder, J. Albrecht, G. Lütjering, Microstructure and mechanical properties of an inertia friction welded INCOLOY alloy 909 – INCONEL alloy 718 joint for rotating applications, *Mater. High Temp.* 23 (2006) 171–177. <https://doi.org/10.1179/mht.2006.011>
- [24] N. L. Richards, M. C. Chaturvedi, Effect of minor elements on weldability of nickel base superalloys, *Int. Mater. Rev.* 45 (2000) 109–129.
<https://doi.org/10.1179/095066000101528331>
- [25] A. Lingenfelter, Welding of Inconel Alloy 718: A Historical Overview, in: *Superalloys 718 Metall. Appl.* 1989, TMS, 1989: pp. 673–683. https://doi.org/10.7449/1989/Superalloys_1989_673-683
- [26] V. T. Gaikwad, M. K. Mishra, V. D. Hiwarkar, R. K. P. Singh, Role of friction time on the joint characteristics of continuous drive friction-welded Inconel 718 and EN24 steel, *J. Mater. Eng. Perform.* 32 (2023) 1660–1670. <https://doi.org/10.1007/s11665-022-07239-9>
- [27] J. N. DuPont, J. C. Lippold, S. D. Kiser, *Welding Metallurgy and Weldability of Nickel-base Alloys*, Wiley, New Jersey, 2009.
<https://doi.org/10.1002/9780470500262>
- [28] Y. S. Kong, M. Cheepu, D. G. Kim, Microstructure and mechanical properties of friction-welded and post-heat-treated Inconel 718, *Trans. Indian Inst. Met.* 73 (2020) 1449–1453.
<https://doi.org/10.1007/s12666-020-01911-1>
- [29] P. Marshall, *Austenitic Stainless Steels: Microstructure and mechanical properties*, Springer Science & Business Media, Springer Dordrecht 1984. ISBN978-0-85334-277-9
- [30] P. E. Schweitzer, *Metallic Materials: Physical, Mechanical, and Corrosion Properties*, CRC Press, New York, 2003. ISBN: 0-8247-0878-4
- [31] M. F. McGuire, *Stainless Steels for Design Engineers*, ASM International, 2008.
<https://doi.org/10.31399/asm.tb.ssde.9781627082860>
- [32] S.-X. Li, Y.-N. He, S.-R. Yu, P.-Y. Zhang, Evaluation of the effect of grain size on chromium carbide precipitation and intergranular corrosion of 316L stainless steel, *Corros. Sci.* 66 (2013) 211–216.
<https://doi.org/10.1016/j.corsci.2012.09.022>
- [33] A. R. Beeravolu, N. K. Babu, M. K. Talari, A. U. Rehman, P. Srirangam, Influence of microstructure and mechanical properties of dissimilar rotary friction welded Inconel to stainless steel joints, *Materials* 16 (2023) 3049. <https://doi.org/10.3390/ma16083049>
- [34] V. Ajay, M. Naveen Kumar, N. Kishore Babu, T. Mahesh Kumar, K. Vamshi Krishna, G. Madhusudan Reddy, Rotary friction welding of Inconel 718-AISI 304 stainless steel dissimilar joint, *Mater. Sci. Technol.* 39 (2023) 1950–1960.
<https://doi.org/10.1080/02670836.2023.2187146>
- [35] P. Pavan, M. K. Talari, N. K. Babu, A. U. Rehman, P. Srirangam, Effect of heat treatment on the microstructure and mechanical properties of rotary friction welded dissimilar IN718 to SS304L alloys, *Appl. Sci.* 13 (2023) 3584. <https://doi.org/10.3390/app13063584>
- [36] P. Anitha, M. C. Majumder, V. Saravanan, S. Rajakumar, Microstructural characterization and mechanical properties of friction-welded IN718 and SS410 dissimilar joint, *Metallogr. Microstruct. Anal.* 7 (2018) 277–287. <https://doi.org/10.1007/s13632-018-0447-0>

- [37] J. Alex Anandaraj, S. Rajakumar, V. Balasubramanian, V. Petley, Investigation on mechanical and metallurgical properties of rotary friction welded In718/SS410 dissimilar materials, *Mater. Today Proc.* 45 (2021) 962–966.
<https://doi.org/10.1016/j.matpr.2020.03.040>
- [38] N. Y. Kim, J. H. Kim, Y. S. Kong, J. W. Yoon, J. T. Yeom, D. G. Lee, N. K. Park, The effect of post weld heat treatment on mechanical properties of friction-welded alloy 718 and SNCRW stainless steel, *Adv. Mater. Res.* 26–28 (2007) 511–514.
<https://doi.org/10.4028/www.scientific.net/AMR.26-28.511>
- [39] M. Cheepu, W. S. Che, Characterization of interfacial microstructure in friction welds between Inconel 718 and SM45C steel, *Trans. Indian Inst. Met.* 73 (2020) 1567–1571.
<https://doi.org/10.1007/s12666-020-01921-z>
- [40] J. T. Tharappel, J. Babu, Welding processes for Inconel 718- A brief review, *IOP Conf. Ser. Mater. Sci. Eng.* 330 (2018) 012082.
<https://doi.org/10.1088/1757-899X/330/1/012082>
- [41] K. Devendranath Ramkumar, S. D. Patel, S. Sri Praveen, D. J. Choudhury, P. Prabakaran, N. Arivazhagan, M. A. Xavier, Influence of filler metals and welding techniques on the structure–property relationships of Inconel 718 and AISI 316L dissimilar weldments, *Mater. Des.* 62 (2014) 175–188.
<https://doi.org/10.1016/j.matdes.2014.05.019>
- [42] Y. F. Li, S. T. Hong, H. Choi, H. N. Han, Solid-state dissimilar joining of stainless steel 316L and Inconel 718 alloys by electrically assisted pressure joining, *Mater. Charact.* 154 (2019) 161–168.
<https://doi.org/10.1016/J.MATCHAR.2019.06.005>
- [43] A. Bansal, A. K. Sharma, S. Das, P. Kumar, On microstructure and strength properties of microwave welded Inconel 718/stainless steel (SS-316L), *J. Mater. Des. Appl.* 230 (2016) 939–948.
<https://doi.org/10.1177/1464420715589206>
- [44] A. Hinojos, J. Mireles, A. Reichardt, P. Frigola, P. Hosemann, L. E. Murr, R. B. Wicker, Joining of Inconel 718 and 316 stainless steel using electron beam melting additive manufacturing technology, *Mater. Des.* 94 (2016) 17–27.
<https://doi.org/10.1016/J.MATDES.2016.01.041>
- [45] S. V. Lalam, G. M. Reddy, T. Mohandas, M. Kamaraj, B. S. Murty, Continuous drive friction welding of Inconel 718 and EN24 dissimilar metal combination, *Mater. Sci. Technol.* 25 (2009) 851–861.
<https://doi.org/10.1179/174328408X369384>
- [46] A. P. Ramesh, M. Subramaniyan, P. Eswaran, Review on friction welding of similar/dissimilar metals, *J. Phys. Conf. Ser.* 1362 (2019) 012032.
<https://doi.org/10.1088/1742-6596/1362/1/012032>
- [47] N. Ozdemir, Investigation of the mechanical properties of friction-welded joints between AISI 304L and AISI 4340 steel as a function of rotational speed, *Mater. Lett.* 59 (2005) 2504–2509.
<https://doi.org/10.1016/j.matlet.2005.03.034>
- [48] İ. Kirik, N. Özdemir, Friction welding machine manufacturing used in the automotive industry and joining of AISI 1040/AISI204L steel pairs with different properties using friction energy, *Technol. Appl. Sci.* 7 (2012) 60–74. (in Turkish)
<https://dergipark.org.tr/en/pub/nwsatecapsci/issue/20170/213911>
- [49] ASTM E407-07, Standard Practice for Microetching Metals and Alloys, ASTM International, n.d.
<https://doi.org/10.1520/E0407-07>
- [50] ASTM E92-17, Standard Test Methods for Vickers Hardness and Knoop Hardness of Metallic Materials, (n.d.).
<https://doi.org/10.1520/E0092-17>
- [51] ASTM E8/E8M-22, Standard Test Methods for Tension Testing of Metallic Materials, (n.d.).
https://doi.org/10.1520/E0008_E0008M-22
- [52] T. J. Lienert, ed., *ASM handbook. 6A: Welding: Fundamentals and Processes*, ASM International, Materials Park, Ohio, 2011. ISBN-13: 978-1-61503-133-7
- [53] G. E. Totten, *Steel Heat Treatment: Metallurgy and Technologies*, CRC Press, Boca Raton, 2006.
<https://doi.org/10.1201/NOF0849384523>
- [54] E. O. Ezugwu, Z. M. Wang, A. R. Machado, The machinability of nickel-based alloys: A review, *J. Mater. Process. Technol.* 86 (1999) 1–16.
[https://doi.org/10.1016/S0924-0136\(98\)00314-8](https://doi.org/10.1016/S0924-0136(98)00314-8)
- [55] N. Switzner, Z. Yu, M. Eff, T. Lienert, A. Fonseca, Microstructure and mechanical property variations within inertia friction-welded joints of stainless steel to steel, *Int. J. Adv. Manuf. Technol.* 95 (2018) 4327–4340.
<https://doi.org/10.1007/s00170-017-1568-3>
- [56] B. Skowrońska, T. Chmielewski, M. Kulczyk, J. Skiba, S. Przybysz, Microstructural investigation of a friction-welded 316L stainless steel with ultrafine-grained structure obtained by hydrostatic extrusion, *Materials* 14 (2021) 1537.
<https://doi.org/10.3390/ma14061537>
- [57] P. Sathiyaa, S. Aravindan, A. N. Haq, Some experimental investigations on friction welded stainless steel joints, *Mater. Des.* 29 (2008) 1099–1109.
<https://doi.org/10.1016/j.matdes.2007.06.006>
- [58] O. A. Hilders, N. Zambrano, R. Caballero, Microstructure, strength, and fracture topography relations in AISI 316L stainless steel, as seen through a fractal approach and the Hall-Petch law, *Int. J. Met.* 2015 (2015) 624653.
<https://doi.org/10.1155/2015/624653>
- [59] G. A. Muhamed, S. Gündüz, M. A. Erden, D. Taştumur, Dynamic strain aging behaviour in AISI 316L austenitic stainless steel under as-received and as-welded conditions, *Metals* 7 (2017) 362.
<https://doi.org/10.3390/met7090362>